NANO · MICRO small
www.small-journal.com

Interfacial Nanoinjection-Based Nanoliter Single-Cell Analysis

Juanli Yun, Xiaowei Zheng, Peng Xu, Xu Zheng, Jingyue Xu, Chen Cao, Yusi Fu, Bingxue Xu, Xin Dai, Yi Wang, Hongtao Liu, Qiaolian Yi, Yaxin Zhu, Jian Wang, Li Wang, Zhiyang Dong, Li Huang, Yanyi Huang,* and Wenbin Du**

Single-cell analysis offers unprecedented resolution for the investigation of cellular heterogeneity and the capture of rare cells from large populations. Here, described is a simple method named interfacial nanoinjection (INJ), which can miniaturize various single-cell assays to be performed in nanoliter water-in-oil droplets on standard microwell plates. The INJ droplet handler can adjust droplet volumes for multistep reactions on demand with high precision and excellent monodispersity, and consequently enables a wide range of single-cell assays. Importantly, INJ can be coupled with fluorescence-activated cell sorting (FACS), which is currently the most effective and accurate single-cell sorting and isolation method. FACS-INJ pipelines for high-throughput plate well-based single-cell analyses, including single-cell proliferation, drug-resistance testing, polymerase chain reaction (PCR), reverse-transcription PCR, and whole-genome sequencing are introduced. This FACS-INJ pipeline is compatible with a wide range of samples and can be extended to various single-cell analysis applications in microbiology, cell biology, and biomedical diagnostics.

1. Introduction

This paper describes interfacial nanoinjection (INJ), a simple microfluidic droplet-handling system developed for multistep nanoliter assays on standard 96- or 384-well plates, and a simple pipeline that couples INJ and fluorescence-activated cell sorting (FACS) for single-cell analyses with high versatility, high throughput, and low cost. Recent research advances have promoted the study of biological systems with respect to their physiological phenotypes,[1] genomics,[2,3] transcriptomics,[4] epigenomics,[5] proteomics,[6] multiomics,[7] and biodiversity[8] at the single-cell level. Single-cell analysis allows the fundamental understanding of cell-to-cell heterogeneity and provides unprecedented resolution in complex biological systems, especially those from rare cell types or uncultivated microbes.[9,10] However, current approaches for single-cell analysis usually involve complicated processes and instruments, require the use of microfabrication devices, and are cost-prohibitive for common laboratories.

In general, a single-cell analysis process can be divided into three major steps: single-cell isolation, reaction, and measurement. Single-cell isolation is the prerequisite step for single-cell analysis. Several systems have been commercialized with the capability of performing single-cell analysis with submicroliter to nanoliter volumes.[11,12] However, these systems are limited to certain cell types or confined to only one specific application or workflow. Microfluidic devices enable ultrahigh throughput isolation, reaction, and analysis of single cells.[8,13,14] However, most microfluidic devices lack standardization which affects its world-to-chip interconnections and flexibility in coping with changes in applications. Currently,

Dr. J. L. Yun, Dr. X. W. Zheng, Dr. P. Xu,[+] J. Y. Xu, B. X. Xu, Dr. X. Dai, Y. Wang, H. T. Liu, Q. L. Yi, Y. X. Zhu, Dr. J. Wang, Dr. L. Wang, Prof. Z. Y. Dong, Prof. L. Huang, Prof. W. B. Du
State Key Laboratory of Microbial Resources
Institute of Microbiology
Chinese Academy of Sciences
Beijing 100101, China
E-mail: huangl@im.ac.cn; wenbin@im.ac.cn

Prof. X. Zheng
State Key Laboratory of Nonlinear Mechanics
Institute of Mechanics
Chinese Academy of Sciences
Beijing 100190, China

The ORCID identification number(s) for the author(s) of this article can be found under https://doi.org/10.1002/smll.201903739.

[+]Present address: Bioengineering and Therapeutic Sciences, University of California, San Francisco, San Francisco, CA 94158, USA
[++]Present address: Lewis-Sigler Institute for Integrative Genomics, Princeton University, Princeton, NJ 08540, USA

J. Y. Xu, B. X. Xu, H. T. Liu, Q. L. Yi, Prof. Z. Y. Dong, Prof. L. Huang, Prof. W. B. Du
College of Life Sciences
University of the Chinese Academy of Sciences
Beijing 100049, China

Dr. C. Cao,[++] Dr. Y. S. Fu, Prof. Y. Y. Huang
Biomedical Pioneering Innovation Center (BIOPIC)
Beijing Advanced Innovation Center for Genomics (ICG)
College of Engineering
School of Life Sciences
Peking-Tsinghua Center for Life Sciences
Peking University
Beijing 100871, China
E-mail: huang@pku.edu.cn

Prof. W. B. Du
Savaid Medical School
University of the Chinese Academy of Sciences
Beijing 100049, China

DOI: 10.1002/smll.201903739

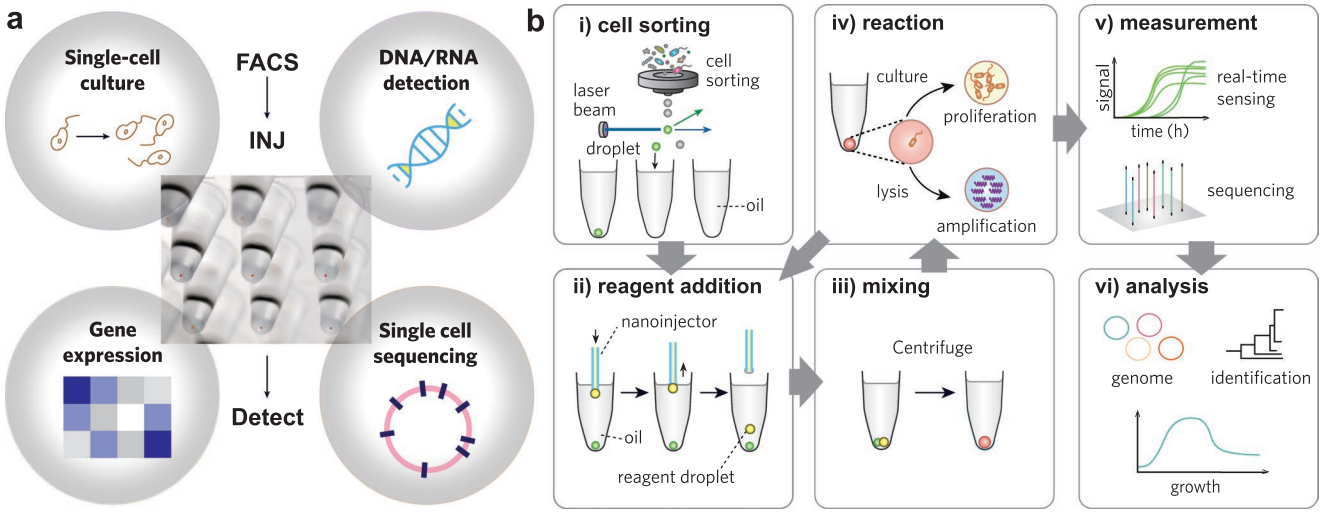

Figure 1. a) FACS-INJ pipeline and its single-cell analysis applications. b) General single-cell assay processed by FACS-INJ. i) single cells are sorted by FACS (MoFlo XDP, Beckman Coulter) into microwells preloaded with mineral oil. ii) Nanoliter volumes of reagents are added to the microwells by the INJ. iii) Droplets are coalesced in microwells by centrifugation (MINIP-2500, Miulab, Shanghai, China). iv) Droplets are incubated in different conditions for various single-cell assays, such as live-cell proliferation and molecular analysis. v) Single-cell assay results are measured by fluorescence readers (EnSpire, Perkin Elmer; or Viia7 Real-Time PCR thermocycler, Applied Biosystems), and amplified nucleic acids are subjected to next-generation sequencing. vi) Data analysis and interpretation.

flow cytometry, especially FACS, remains as the most widely used single cell isolation method. FACS enables high-throughput single-cell sorting with multiple dimensions and reduces contamination caused by the codeposition of extracellular contaminants.[15,16] Moreover, FACS can sort single cells into standard microwell plates for single-cell cultivation, detection, or amplification, and the results can be read out using microscopes or plate readers. However, FACS is not compatible with state-of-art microfluidic platforms, and most of these FACS-based single-cell assays are performed at the microliter level, which is costly when a large number of single cells have to be studied. Scaling down a single-cell reaction to the nanoliter level is helpful to reduce the cost, minimize contamination,[17,18] avoid dilution of minute amounts of cellular components (e.g., DNA, RNA, protein, and secretions), and reduce the assay time. Hitherto, a major unmet need is the lack of a miniaturized liquid handling system that can interface the upstream FACS and downstream measurements for high-throughput nanoliter single-cell assays. In this paper, we introduce INJ, which handles nanoliter droplets with high precision and allows multistep nanoliter assays on standard microwell plates. We coupled INJ with FACS and different commercial fluorescence readers and demonstrated the performance of the platform in various single-cell phenotypic and genotypic analyses, as well as whole-genome amplification (WGA). We believe that the FACS-INJ platform can provide simple, reliable, flexible, and versatile features for various single-cell analyses of both prokaryotic and eukaryotic cells.

2. Results

2.1. The FACS-INJ Pipeline

The overview workflow of the FACS-INJ system is shown in **Figure 1**a. It allows live-cell proliferation or cell-lysate analysis such as DNA and RNA level gene amplification and detection (Figure 1a). Figure 1b illustrates the detailed procedures of single cell analyses with the FACS-INJ pipeline. First, single cells are sorted into oil-filled wells by FACS; afterward, nanoliter droplets containing different reagents are sequentially added to the wells by the INJ droplet handler (Figure S1, Supporting Information). A brief centrifugation step moves all the droplets to the well bottom, exerts kinetic energy to bring the droplets together, and forces the coalescence of droplets. The measurements of single-cell assays on microwell plates are performed by commercial fluorescence readers and followed by data analysis.

2.2. Nanoliter Droplet Handling with INJ

A simple automated droplet handler that applies the INJ technique was established using commercially available components (Figure S1, Supporting Information). The system consists of a syringe pump with a syringe, Teflon tubing attached to the syringe pump, a short fused-silica capillary sealed to the outlet of the tubing and vertically mounted to the Z translation stage, and an oil-filled microwell plate mounted on an XY translation stage. To use the droplet handler, the syringe pump is prefilled with mineral oil, and microliters of reagents are aspirated into the Teflon tubing. The XY and Z stages are operated to insert the capillary tip into the oil-filled microwell, and nanoliter droplets down to 1 nL in volume can be injected into the oil by positive displacement of the pump. Then, the tip is pulled out of the surface of the oil in the well, and the droplet is pinched off the tip by the interfacial confinement and settles to the bottom of the well (**Figure 2**a,b and Movie S1, Supporting Information). The whole process is automated by a LabVIEW computer program, and the volume of droplets down to 1 nL can be customized for each well of the plate (Figure 2c and Movie S1,

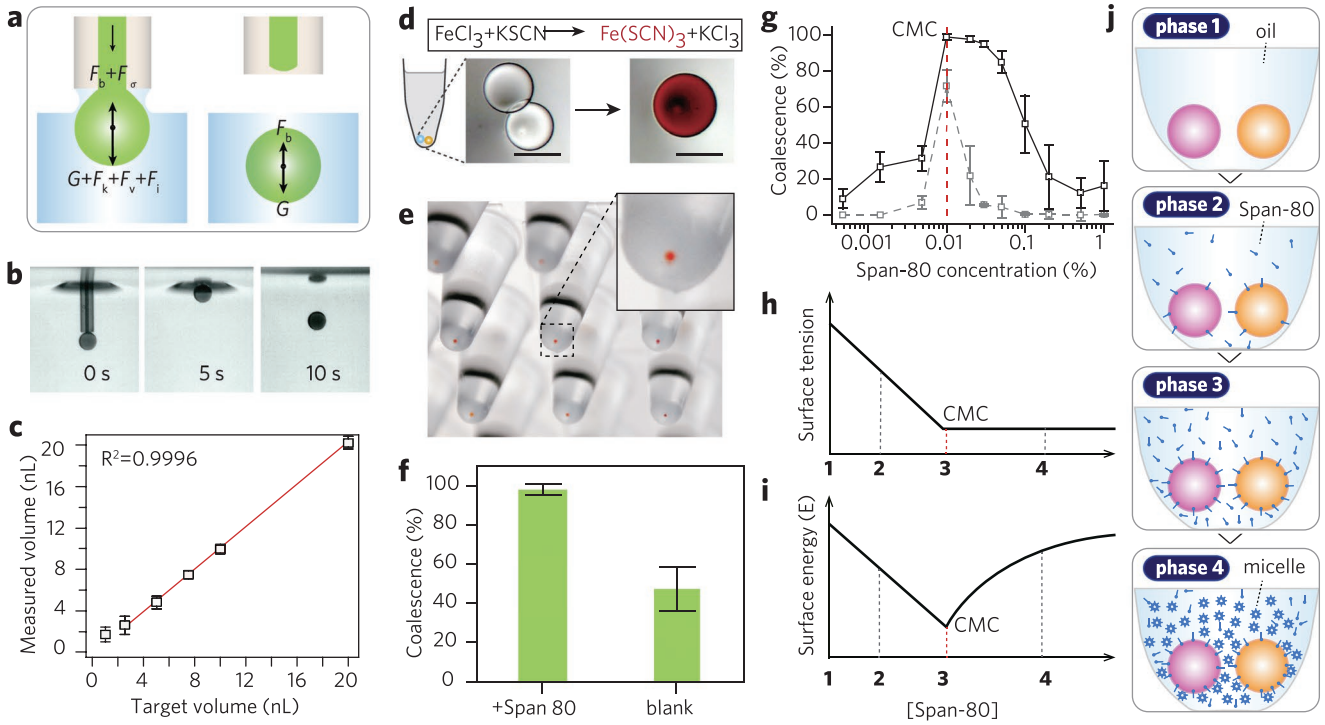

Figure 2. INJ performance in nanoliter droplet handling. a) Schematic illustration of the mechanism of droplet pinch-off from the tip of the capillary by INJ. b) Photomicrographs illustrating the generation of a 1 nL droplet by INJ at the mineral oil interface. c) Linear regression of injected and measured droplet volumes in the range of 1–20 nL. The error bars are the standard deviation of 25 replicates. d) Photomicrographs illustrating the coalescence of $FeCl_3$ and KSCN droplets in microwells after centrifugation, initiating the chromogenic reaction to produce an $Fe(SCN)^{2+}$ complex (red). Bars represent 200 µm. e) The coalescence of FACS-sorted droplets (≈2 nL, 0.1 M KSCN) with preloaded droplets (20 nL, 0.5 M $FeCl_3$) on a 96-well plate visualized by the chromogenic reaction. f) The coalescence ratio of FACS-sorted and preloaded droplets with or without the addition of Span-80 (0.01%). Error bars indicate the standard deviation for three 96-well plates ($n = 288$). g) Relationship between coalescence ratio and Span-80 concentration in mineral oil before (gray dashed line) and after centrifugation (solid black line). A consistent maximum coalescence rate was reached at 0.01–0.02% v/v Span-80 (red dashed line). The error bars are the standard deviations of three 96-well plates ($n = 288$). h–j) Schematic illustrations of the CMC-dependent coalescence of nanoliter droplets in microwells.

Supporting Information). The use of mineral oil prevents nanoliter droplet evaporation and contamination and provides a biocompatible environment for various single-cell analyses. 96- or 384-well plates with V-shaped bottoms allows convergence of multiple droplets at the bottom of the well upon centrifugation, yielding a coalescence ratio of 99.2% ($n = 288$) for 5 nL droplets (Figure 2d,g), and a 97.9% ($n = 288$) coalescence ratio of the FACS-sorted droplets (≈2 nL) with a preloaded 20 nL droplets (Figure 2e,f). More details for optimization and performance of droplet handling are provided in the Supporting Information.

2.3. Single-Cell Phenotypic Analysis

To demonstrate that the FACS-INJ pipeline is compatible with the single-cell phenotypic analysis, we selected *Escherichia coli* (*E. coli*) ATCC 25922 as a model strain for single-cell culture and measurement of the minimum inhibitory concentration (MIC) at the single-cell level. We used resazurin as a sensitive fluorescence indicator for bacterial proliferation.[19] We optimized the droplet volume for cell cultivation in Luria broth containing 0.01% w/v resazurin (Figure S3, Supporting Information) and found that a 100 nL droplet volume yielded stable fluorescence profiles for dynamic *E. coli* single-cell growth monitoring (**Figure 3**b and Figure S3, Supporting Information). Next, we sorted single *E. coli* cells into 384-well plates and performed antimicrobial susceptibility

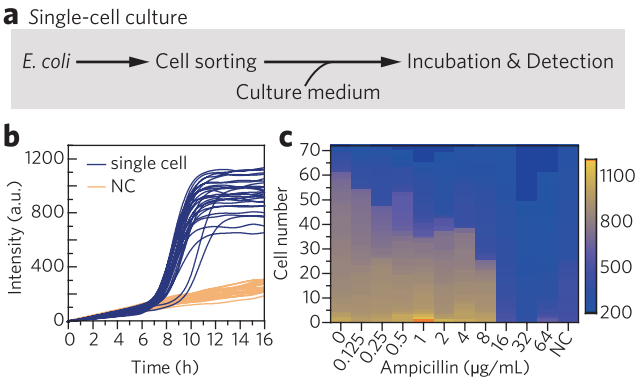

Figure 3. Single-cell cultivation and AST. a) FACS-INJ single-cell culture workflow. b) The growth curves of single *E. coli* cells. Both single-cell and negative control results include 103 replicates. c) The heatmap shows the endpoint fluorescence intensity (16 h) of 72 replicate wells at different antibiotic (ampicillin) concentrations. NC, no-cell control wells. The increased fluorescence intensity indicates increased cell growth at the corresponding ampicillin concentration. There is no growth when the fluorescence intensity is less than 500.

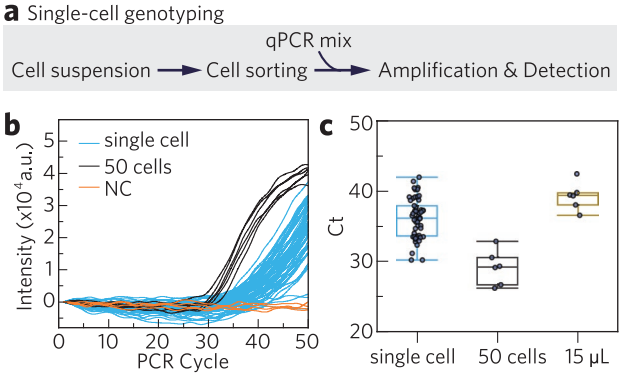

Figure 4. a) FACS-INJ workflow for single-cell genotyping based on Taqman PCR. b) Taqman qPCR amplification curves and c) *Ct* value comparison for single cells in 800 nL ($n = 60$), 50 cells in 800 nL ($n = 6$), and single cells in 15 µL ($n = 6$) volumes.

testing (AST) on the single cells to measure the MIC of ampicillin against *E. coli*. As shown in Figure 3c, the percentage of growth of single cells decreased with increasing concentrations of ampicillin, and no cells grew in the presence of 16 µg mL^{-1} ampicillin, which was determined as the MIC. The single-cell AST result is consistent with the conventional AST result on microwell plates. In comparison, our method consumes 2000 times fewer reagents than conventional plate assays (200 µL) and, more importantly, provides population-level statistical analysis to characterize physiological responses of individual cells to culture conditions, antibiotics, and chemicals.

2.4. Single-Cell Genotypic Analysis

To enable single-cell genotyping and pathogen detection, we used the FACS-INJ system to perform polymerase chain reaction (PCR)-based nucleic acid amplification of antibiotic-resistance genes of the pathogenic bacteria *Acinetobacter baumannii* (**Figure 4**a). In total, 104 single cells were sorted and amplified by using quantitative real-time PCR with *bla*$_{\text{OXA-51}}$ gene-specific primers and a TaqMan probe. The amplification resulted in 188 bp amplicons for the *bla*$_{\text{OXA-51}}$ targeted site, which encodes beta-lactamase in *A. baumannii*.

We scaled down the PCR volume to 800 nL, as shown in the real-time fluorescence curves in Figure 4b. The target sequences were amplified in 59 out of 104 reactions. In order to confirm the specificity of the *bla*$_{\text{OXA-51}}$ gene detection, we also set up negative controls using *Pseudomonas aeruginosa* PAO1 single cell lysate and no amplification was observed in 80 replicates, indicating the specificity of our antibiotic resistant gene measurement. Compared with the conventional PCR in a 15 µL volume ($n = 15$), the nanoliter reaction shows higher sensitivity (Figure 4c) with a lower *Ct* value ($\Delta Ct = 2.23$, based on the mean *Ct* value of each volume). The overall single-cell PCR amplification success rate was 56.7%, which is consistent with previous studies.[20,21] We also ran a cell number-based amplification for comparison with the single-cell PCR. The 10-cell PCR showed an overall 91.7% (44 of 48) success rate, the 50-cell PCR amplification showed an overall 96.9% (31 of 32) success rate, and no amplification was detected in the no-cell control reactions (Figure 4b). The ΔCt between 10 cells and single cells was 5.56 ± 1.0, and that between 50 cells and single cells was 6.93 ± 0.3. As FACS allows selective sorting of rare pathogens in complex samples such as blood and cerebrospinal fluid, the single-cell PCR tests can provide culture-free rapid identification of pathogenic bacteria and fungi as well as their drug resistance genes of infectious diseases at early stage.

2.5. Single-Cell Gene Expression

To demonstrate the single-cell gene expression analysis capability of FACS-INJ, we measured the inflammatory response of mouse macrophage RAW264.7 cells treated with bacterial lipopolysaccharide (LPS) at the RNA level with multiplexed one-step reverse-transcription PCR (RT-PCR). Previous studies have shown that LPS, a major outer membrane component of gram-negative bacteria, is an endotoxin that induces the macrophage inflammatory response to release proinflammatory cytokines, including interleukin-1β (IL-1β),[22] which is indicated by the upregulation of the expression of the IL-1β coding gene. To measure IL-1β gene expression with or without LPS treatment, we designed a duplexed RT-PCR system to detect the expression of the IL-1β gene and the housekeeping gene hypoxanthine guanine phosphoribosyltransferase (HPRT) as an internal reference. Single RAW264.7 cells with or without LPS treatment were sorted and merged with the RT-PCR mix for the real-time RT-PCR analysis (**Figure 5**a). In the optimal reaction volume of 600 nL (Figure 5a and Figure S4, Supporting Information), HPRT showed consistent expression in both LPS-treated and untreated cells, while IL-1β expression in single cells treated with LPS was significantly upregulated compared to that of untreated cells (Figure 5b–d). This FACS-INJ-based single-cell RT-PCR can be applied to analyze the gene expression of mammalian cells, plant cells, and microorganisms.

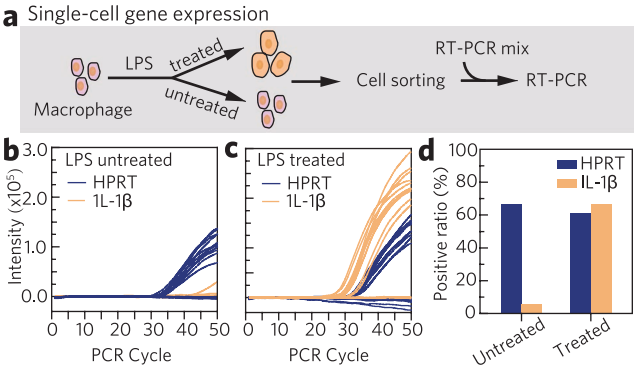

Figure 5. a) Single-cell gene expression workflow based on FACS. The mouse macrophage cell line RAW264.7 was treated with either LPS or medium, and the inflammatory response of a single cell was measured by one-step RT-PCR using the FACS-INJ system. b,c) RT-PCR detection of HPRT and IL-1β gene expression levels in macrophages treated with b) medium or c) 100 ng mL^{-1} LPS for 16 h. d) Single-cell IL-1β gene expression profiling with and without LPS treatment.

2.6. Single-Cell Sequencing

To enable the single-cell sequencing of uncultivatable microorganisms, we developed a single-cell multiple displacement amplification (MDA) pipeline based on FACS-INJ, evaluated its performance with a benchmark strain, and applied it to the WGA of deep-sea microorganisms. MDA has been widely used for single-cell WGA due to its high recovery rate and accuracy.[23] As shown in **Figure 6**a, the workflow involves sorting, lysis, neutralization, amplification, and phylogenetic identification steps. These steps of the optimal procedure require the addition of nanoliter droplets of the corresponding reagent ranging from 20 to 300 nL in volume, with a final reaction volume of 360 nL. SYBR Green was added to the amplification mix to allow real-time monitoring of single-cell MDA and the selection of positive reactions for subsequent sequencing and phylogenetic identification (Figures 1 and 6a).

To optimize the single-cell MDA and control for contamination, we evaluated the performance of a series of volumes ranging from 160 to 1060 nL using *Sulfolobus* sp. A20 (an archaeal strain isolated from an acidic hot spring in Laguna Fumarólica, Costa Rica[24]) as the benchmark strain (Figure 6b–d). For each volume, we used 100 cells as positive controls and no cells as negative controls. Based on the critical point (Cp) of the real-time amplification curves of the single cells and controls, we obtained an optimal reaction volume of 360–560 nL, for which Cps from single cells and positive controls (<3 h) can be distinguished from those of the negative controls (>3 h), indicating successful amplification of a single cell without contamination. We found that reaction volumes greater than 660 nL introduce serious contamination (Figure 6b and Figures S5 and S6, Supporting Information). These results confirm that single-cell MDA in reduced nanoliter volumes can effectively decrease the risks of the off-target amplification of contaminants.[3,17]

To further assess the performance of single-cell MDA, we sent the products of successful reactions in different volumes for sequencing and obtained ≈600 million reads from each amplification product to produce single-cell genome assemblies. The results revealed that the average whole-genome

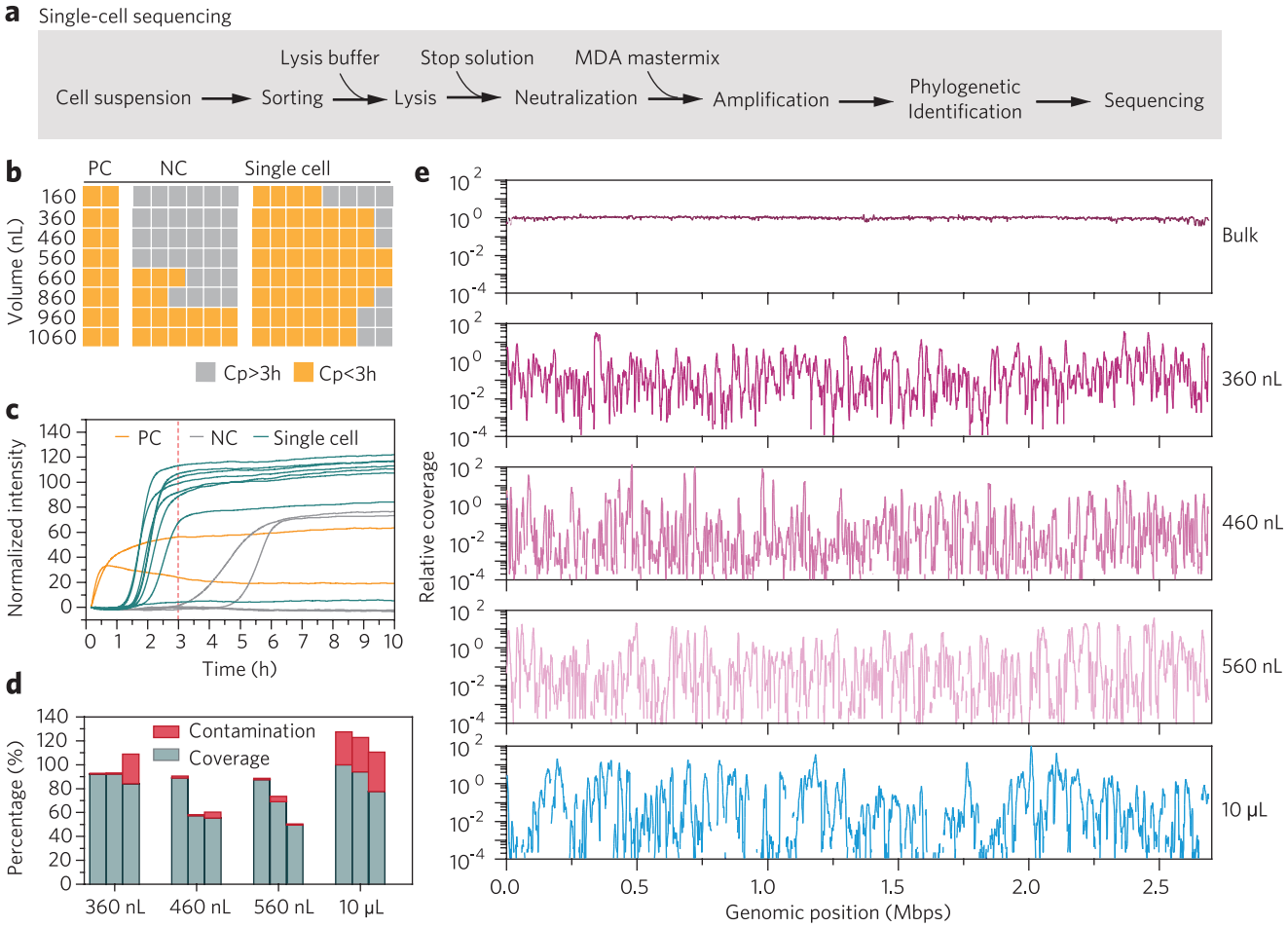

Figure 6. Single-cell whole-genome MDA amplification with the benchmark strain *Sulfolobus* sp. A20. a) Workflow. b) Optimization of the MDA reaction volume from 110 to 1060 nL. Each square represents one replicate for each reaction volume. PC indicates replicates with 100 cells, and NC is the negative control without cells. c) Real-time fluorescence curves for single *Sulfolobus* sp. A20 cell MDA in a 360 nL reaction volume. d) Genome coverage and contamination of each assembly. Error bars are the standard deviation of three replicates. e) The evenness of representative single-cell assemblies in different reaction volumes.

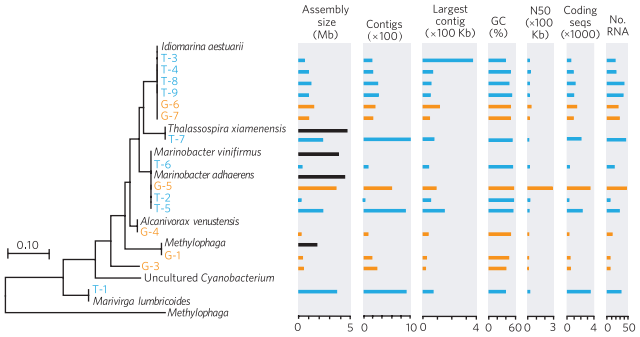

Figure 7. Phylogenetic assignment and annotation details of Southwest Indian Sea sediment single-cell assemblies. Blue and orange bars represent single cells from sedimentary Tombarthite (T) and a sediment core collected using a gravity column sampler (G), respectively. Black bars represent reference genomes in the National Center for Biotechnology Information database.

coverage for 360, 460, and 560 nL single-cell MDA was 79.0%, 55.4%, and 61.3%, respectively. The genome coverage was not significantly different from that obtained in 10 µL reaction volumes (65.2%). However, the contamination ratio for the nanoliter MDA in the range of 360–560 nL was less than 5% (Figure 6d), which is significantly better than that of the 10 µL volume reactions (Figure 6d and Table S2, Supporting Information). Moreover, MDA in nanoliter volumes presented better evenness of WGA than that in the 10 µL volume (Figure 6e and Figure S7, Supporting Information), which is consistent with the results of previous microfluidic-based single-cell MDA studies.[2,3,17,25]

To assess the performance of single-cell MDA in retrieving the whole genome sequences of uncultivated microbes, two deep-sea sediment samples from the Southwest Indian Ocean, including a sedimentary Tombarthite (T) and a sediment core collected with a gravity column sampler (G), were used for single-cell MDA at optimal 360–560 nL volumes. After phylogenetic identification, 15 single-cell MDA products (9 from T and 6 from G samples) were sequenced and each yielded ≈2 Gb paired-end reads. As shown in **Figure 7**, the sizes of the assemblies ranged from 0.21 to 3.67 Mbp, and the genome completeness was estimated to vary from 6.04% to 73.5% (Figure S8a, Supporting Information). Compared to previous single-cell MDA methods,[3,10,25] the FACS-INJ pipeline produces comparable assembly size and completeness with markedly lower contamination levels (<5%), indicating that our single-cell WGA is robust and compatible with environmental samples. We also found large numbers of carbohydrate-active enzymes (CAZymes) in all single-cell genome assemblies (Figure S8b, Supporting Information), indicating that these microbes potentially function in carbon cycling in deep oceans.

3. Discussion

Here, we describe FACS-INJ, a new platform that combines INJ droplet handling with FACS for high-throughput single-cell analyses in nanoliter volumes. FACS provides multidimensional selectivity of target cells as well as compatibility with various types of single-cell assays (Figure 1a). INJ provides many advantages over other microfluidic methods. First, only a syringe pump and a compact automated translation stage are required for the assembly of the INJ droplet handler, which can be easily established in common laboratories with commercially available components. Second, droplets of volumes down to 5 nL can be generated with high accuracy on demand (Figure 2c) in standard well plates. Third, multistep assays can be performed in nanoliter volumes by sequential INJ of nanoliter droplets of different reagents, followed by efficient coalescence by centrifugation and simple measurement gathering using fluorescence plate readers or real-time PCR machines (Figure 1b and Figure S1, Supporting Information).

The mechanism of droplet pinch-off from the tip of the capillary by INJ is similar to that of our previously reported interfacial emulsification method,[26,27] which continuously generates monodisperse picoliter to nanoliter droplets at throughput speeds of 50 to 500 droplets per second and has been used for digital nucleic acid amplification,[28] polymeric microparticle synthesis,[29] and AST.[30] Briefly, at the very moment the capillary moves out of the oil phase, several forces, including the water–oil interfacial tension F_σ, the viscous drag force F_v, the gravity G, the buoyancy F_b, the kinetic force F_k, and the interfacial confinement force F_i, affect the detachment of the droplet. Among these forces, the confinement force of the water–oil interface, originating from the interfacial tension resisting deformation of the interface during the elevation of the capillary, is the decisive force that overcomes all barrier forces (including F_σ and F_b) against detachment.[26] We evaluate that the force F_i is much larger than the barrier forces $F_\sigma + F_b$, which makes the droplet detachment easy and reproducible. The droplet then settles to the bottom of the well.

The coalescence of nanoliter droplets in microwell plates, which is achieved by the combined effects of the surfactant Span-80 and centrifugation, is the key for the success of multistep single-cell assays. The droplet coalescence ratio at different Span-80 concentrations before and after centrifugation was evaluated by the chromogenic reaction of two 5 nL droplets (Figure 2g). Notably, centrifugation is necessary for fast coalescence (1 min), as it provides kinetic energy for the droplets in the bottom of a microwell to collide with each other, which allows for robust high-throughput analysis. The addition of Span-80 dramatically reduces the surface tension to enhance the coalescence ratio at the critical micelle concentration (CMC), which is 0.01–0.02% v/v (Figure 2d–j). This finding indicates a CMC-dependent coalescence. Generally, the coalescence ratio of droplets is determined by the change in surface energy (Figure 2h,i).

As the Span-80 concentration increases from 0 to the CMC (phase 1–3, Figure 2j), the surface tension gradually decreases, as does the surface energy (E) of the system, which is defined as $n\sigma A$ (where n is the number of droplets in a microwell, $A = 4\pi r^2$ is the surface area of a single droplet). As a result, the coalescence ratio reaches its highest value, which is up to 99.2% with centrifugation, as shown in Figure 2g. When the concentration of Span-80 exceeds the CMC, the surfactant molecules form micelles in the oil solution rather than staying at the interfacial layer of the droplet. In contrast, these micelles in the oil solution prevent the coalescence of the droplets, as they exist between the droplet surfaces and increase the surface energy

($E = nA + A_m$, where A_m is the total surface of the micelles in the oil solution). The blockage effect of these micelles is not fully eliminated by centrifugation, as shown by the lower coalescence ratio than that observed at CMC (phase 4, Figure 2j).

Despite the convenient manipulation and accuracy, FACS-INJ is compatible with most single-cell assays at minimized volume. For example, we used the platform for single-cell phenotypic analysis, genotypic analysis, gene expression analysis, and whole-genome sequencing. All these applications display comparable sensitivity or coverage to that of conventional procedures at microliter volumes, but with greatly reduced reagent consumption and ratios of contamination. The minimized analysis not only is cost-effective but also enables biological research and medical diagnosis based on single-cell analyses. The single-cell AST may provide accurate dose guidance for clinical diagnosis, especially when the available specimen is limited, and reveal the heterogenous drug resistance landscape of pathogens. The detection of DNA and RNA in single cells with PCR and RT-PCR reveals many opportunities in single-cell genotyping, functional identification, and genetic diagnosis of diseases such as sepsis and cancer. Single-cell MDA provides a streamlined workflow for high-throughput single-cell genome sequencing of uncultured microorganisms, as well as circulating tumor cells, thereby may promote the prevalence of individualized precision medicine.

4. Conclusion

In summary, we have developed INJ, a nanoliter droplet handler that allows high-throughput nanoliter assays on microwell plates without a complicated setup or microfabricated devices. Compared with conventional positive-displacement pipetting systems, INJ reduces handling volumes down to the nanoliter level with high precision and reproducibility and is compatible with standard 96- or 384-well plates for automated and high-throughput assays and screening. Importantly, INJ is compatible with commercial FACS and allows us to establish programmable and configurable FACS-INJ pipelines for various single-cell analyses at the nanoliter level. FACS-INJ allows accurate and efficient sorting, isolation, reaction, and measurement of single cells at high-throughput with nanoliter reagent consumption and is versatile, precise, cost-effective, and robust. We recruit FACS as single-cell sorter because FACS allows sorting of particles from 100 nm to several hundred microns, which allows single cell sorting and analysis of viruses,[31] bacteria,[32] yeasts,[33–35] and mammalian cells or multi-cellular organoids. With its high resolution, FACS is capable of distinguishing cells from heterogenous populations based on cell size, shape, cellular content, and phenotypes,[34–36] which shows much higher flexibility than other methods.[37]

Compared with current microfluidic-based single-cell analysis methods which can analyze thousands to tens of thousands of cells in one run, the throughput of FACS-INJ is limited to several hundreds per plate. However, split-pool barcoding method[38] might be integrated to increase the throughput of single cell analysis using FACS-INJ exponentially. Furthermore, the FACS-INJ brings four advantages: i) Compatibility with standardized well plates and detecting facilities; ii) no limitation in number of assay steps and high flexibility to change in demand; iii) high efficiency and specificity in single-cell sorting and selection provided by FACS; iv) no restriction on cell sizes and overcoming limitation of Poisson distribution and multicell events. Compared with other plate-based miniaturization techniques, the FACS-INJ method avoids the disturbance of external forces such as acoustic ejection[11,12] and contamination due to surface contact or evaporation,[39] and allows single-cell assays to be scaled down to tens to hundreds nanoliters on standard well plates.

The detection systems used in this work are common real-time PCR machines or fluorescence plate readers that are widely available. To further reduce the reaction volume of single-cell assays from hundreds of nanoliters to tens of nanoliters, we may use high-resolution and high-sensitivity fluorescence microscopes or customized fluorescence detection systems. We may also extend the detection methods to include electrochemical detectors or chemiluminescence for other applications, such as single-cell immunoassays. In addition to single-cell analysis, FACS-INJ also allows the sorting of different cell types in the same microwell with high selectivity, thus creating great opportunities for cell–cell interaction studies. We believe that the FACS-INJ method is widely applicable for single-cell analysis in microbiology, cell biology, and clinical diagnosis.

5. Experimental Section

See the Supporting Information for the detailed experimental procedures and materials.

Supporting Information

Supporting Information is available from the Wiley Online Library or from the author.

Acknowledgements

J.Y., X.Z., and P.X. contributed equally to this work. W.D., L.H., and Y.H. conceived the project; W.D., L.H., Y.H., J.Y., P.X., X.W.Z., J.X., X.D., J.W., L.W., and Z.D. designed all experiments; W.D., J.Y., P.X., X.W.Z., Y.W., and Q.Y. built and optimized the INJ platform; X.Z. and W.D. built the physical model of INJ; X.W.Z., Y.Z., J.W., and Z.D. collected deep-sea sediment samples; J.Y., P.X., X.W.Z., B.X., Y.W., C.C., and Y.F performed single-cell MDA experiments and bioinformatic analysis; J.X. performed live-cell analysis experiments and gene expression experiments; W.D., J.Y., P.X., X.W.Z., X.Z., and L.H. wrote the manuscript. This work was financially supported by China Ocean Mineral Resources R&D Association (DY135-B2-02), National Natural Science Foundation of China (41977196, 21822408, 21525521, 11832017, 11572335), National Key R&D Program of China (2016YFE0205800, 2016YFC0100900, 2018YFC0310703), the Chinese Academy of Sciences (XDB15040102, QYZDB-SSW-SMC008, QYZDB-SSW-JSC036, KFZD-SW-219-4, XDB22040403), and the State Key Laboratory of Microbial Resources, Institute of Microbiology, Chinese Academy of Sciences (SKLMR-20150602).

Conflict of Interest

The authors declare no conflict of interest.

Keywords

droplet, fluorescence-activated cell sorting, microfluidics, single-cell analysis, single-cell sequencing

Received: July 14, 2019
Revised: September 8, 2019
Published online:

[1] J. H. Levine, E. F. Simonds, S. C. Bendall, K. L. Davis, E. Amir, M. D. Tadmor, O. Litvin, H. G. Fienberg, A. Jager, E. R. Zunder, R. Finck, A. L. Gedman, I. Radtke, J. R. Downing, D. Pe'Er, G. P. Nolan, *Cell* **2015**, *162*, 184.
[2] Y. Marcy, C. Ouverney, E. M. Bik, T. Losekann, N. Ivanova, H. G. Martin, E. Szeto, D. Platt, P. Hugenholtz, D. A. Relman, S. R. Quake, *Proc. Natl. Acad. Sci. USA* **2007**, *104*, 11889.
[3] F. Lan, B. Demaree, N. Ahmed, A. R. Abate, *Nat. Biotechnol.* **2017**, *35*, 640.
[4] D. A. Jaitin, E. Kenigsberg, H. Keren-Shaul, N. Elefant, F. Paul, I. Zaretsky, A. Mildner, N. Cohen, S. Jung, A. Tanay, I. Amit, *Science* **2014**, *343*, 776.
[5] G. Kelsey, O. Stegle, W. Reik, *Science* **2017**, *358*, 69.
[6] J. R. Newman, S. Ghaemmaghami, J. Ihmels, D. K. Breslow, M. Noble, J. L. DeRisi, J. S. Weissman, *Nature* **2006**, *441*, 840.
[7] S. Bian, Y. Hou, X. Zhou, X. Li, J. Yong, Y. Wang, W. Wang, J. Yan, B. Hu, H. Guo, J. Wang, S. Gao, Y. Mao, J. Dong, P. Zhu, D. Xiu, L. Yan, L. Wen, J. Qiao, F. Tang, W. Fu, *Science* **2018**, *362*, 1060.
[8] S. S. Terekhov, I. V. Smirnov, A. V. Stepanova, T. V. Bobik, Y. A. Mokrushina, N. A. Ponomarenko Jr., A. A. Belogurov, M. P. Rubtsova, O. V. Kartseva, M. O. Gomzikova, A. A. Moskovtsev, A. S. Bukatin, M. V. Dubina, E. S. Kostryukova, V. V. Babenko, M. T. Vakhitova, A. I. Manolov, M. V. Malakhova, M. A. Kornienko, A. V. Tyakht, A. A. Vanyushkina, E. N. Ilina, P. Masson, A. G. Gabibov, S. Altman, *Proc. Natl. Acad. Sci. USA* **2017**, *114*, 2550.
[9] C. C. Ooi, G. L. Mantalas, W. Koh, N. F. Neff, T. Fuchigami, D. J. Wong, R. J. Wilson, S. M. Park, S. S. Gambhir, S. R. Quake, S. X. Wang, *PLoS One* **2017**, *12*, e188510.
[10] R. Stepanauskas, E. A. Fergusson, J. Brown, N. J. Poulton, B. Tupper, J. M. Labonte, E. D. Becraft, J. M. Brown, M. G. Pachiadaki, T. Povilaitis, B. P. Thompson, C. J. Mascena, W. K. Bellows, A. Lubys, *Nat. Commun.* **2017**, *8*, 84.
[11] J. Olechno, R. Stearns, R. Ellson, E. Heron, *Innovations Pharm. Technol.* **2006**, *19*, 40.
[12] S. Mora-Castilla, C. To, S. Vaezeslami, R. Morey, S. Srinivasan, J. N. Dumdie, H. Cook-Andersen, J. Jenkins, L. C. Laurent, *J. Lab. Autom.* **2016**, *21*, 557.
[13] D. S. Tawfik, A. D. Griffiths, *Nat. Biotechnol.* **1998**, *16*, 652.
[14] S. S. Terekhov, I. V. Smirnov, M. V. Malakhova, A. E. Samoilov, A. I. Manolov, A. S. Nazarov, D. V. Danilov, S. A. Dubiley, I. A. Osterman, M. P. Rubtsova, E. S. Kostryukova, R. H. Ziganshin, M. A. Kornienko, A. A. Vanyushkina, O. N. Bukato, E. N. Ilina, V. V. Vlasov, K. V. Severinov, A. G. Gabibov, S. Altman, *Proc. Natl. Acad. Sci. USA* **2018**, *115*, 9551.
[15] C. Rinke, J. Lee, N. Nath, D. Goudeau, B. Thompson, N. Poulton, E. Dmitrieff, R. Malmstrom, R. Stepanauskas, T. Woyke, *Nat. Protoc.* **2014**, *9*, 1038.
[16] A. Aharoni, K. Thieme, C. P. Chiu, S. Buchini, L. L. Lairson, H. Chen, N. C. Strynadka, W. W. Wakarchuk, S. G. Withers, *Nat. Methods* **2006**, *3*, 609.
[17] Y. Marcy, T. Ishoey, R. S. Lasken, T. B. Stockwell, B. P. Walenz, A. L. Halpern, K. Y. Beeson, S. M. Goldberg, S. R. Quake, *PLoS Genet.* **2007**, *3*, e155.
[18] C. R. Hutchison, H. O. Smith, C. Pfannkoch, J. C. Venter, *Proc. Natl. Acad. Sci. USA* **2005**, *102*, 17332.
[19] R. Agren, L. Liu, S. Shoaie, W. Vongsangnak, I. Nookaew, J. Nielsen, *PLoS Comput. Biol.* **2013**, *9*, e1002980.
[20] K. Leung, H. Zahn, T. Leaver, K. M. Konwar, N. W. Hanson, A. P. Page, C. C. Lo, P. S. Chain, S. J. Hallam, C. L. Hansen, *Proc. Natl. Acad. Sci. USA* **2012**, *109*, 7665.
[21] R. Tewhey, J. B. Warner, M. Nakano, B. Libby, M. Medkova, P. H. David, S. K. Kotsopoulos, M. L. Samuels, J. B. Hutchison, J. W. Larson, E. J. Topol, M. P. Weiner, O. Harismendy, J. Olson, D. R. Link, K. A. Frazer, *Nat. Biotechnol.* **2009**, *27*, 1025.
[22] S. Guan, H. Feng, B. Song, W. Guo, Y. Xiong, G. Huang, W. Zhong, M. Huo, N. Chen, J. Lu, X. Deng, *Int. Immunopharmacol.* **2011**, *11*, 2194.
[23] F. B. Dean, S. Hosono, L. Fang, X. Wu, A. F. Faruqi, P. Bray-Ward, Z. Sun, Q. Zong, DuY , DuJ , M. Driscoll, W. Song, S. F. Kingsmore, M. Egholm, R. S. Lasken, *Proc. Natl. Acad. Sci. USA* **2002**, *99*, 5261.
[24] X. Dai, H. Wang, Z. Zhang, K. Li, X. Zhang, M. Mora-Lopez, C. Jiang, C. Liu, L. Wang, Y. Zhu, W. Hernandez-Ascencio, Z. Dong, L. Huang, *Front. Microbiol.* **2016**, *7*, 1902.
[25] M. Hosokawa, Y. Nishikawa, M. Kogawa, H. Takeyama, *Sci. Rep.* **2017**, *7*, 5199.
[26] P. Xu, X. Zheng, Y. Tao, W. Du, *Anal. Chem.* **2016**, *88*, 3171.
[27] S. L. Liao, Y. Tao, W. B. Du, Y. P. Wang, *Langmuir* **2018**, *34*, 11655.
[28] Y. Hu, P. Xu, J. Luo, H. He, W. Du, *Anal. Chem.* **2017**, *89*, 745.
[29] S. Liao, Y. He, D. Wang, L. Dong, W. Du, Y. Wang, *Adv. Mater. Technol.* **2016**, *1*, 1600021.
[30] S. L. Liao, X. L. Tao, Y. J. Ju, J. Feng, W. B. Du, Y. P. Wang, *ACS Appl. Mater. Interfaces* **2017**, *9*, 4345.
[31] S. Sokolenko, J. Nicastro, R. Slavcev, M. G. Aucoin, *Cytometry, Part A* **2012**, *81A*, 1031.
[32] L. Wu, Y. Song, T. Luan, L. Ma, L. Su, S. Wang, X. Yan, *Biosens. Bioelectron.* **2016**, *86*, 102.
[33] E. T. Boder, K. D. Wittrup, *Nat. Biotechnol.* **1997**, *15*, 553.
[34] H. Zhang, A. Torkamani, T. M. Jones, D. I. Ruiz, J. Pons, R. A. Lerner, *Proc. Natl. Acad. Sci. USA* **2011**, *108*, 13456.
[35] A. Rajpal, N. Beyaz, L. Haber, G. Cappuccilli, H. Yee, R. R. Bhatt, T. Takeuchi, R. A. Lerner, R. Crea, *Proc. Natl. Acad. Sci. USA* **2005**, *102*, 8466.
[36] R. A. Lerner, *Angew. Chem., Int. Ed.* **2006**, *45*, 8106.
[37] A. Gross, J. Schoendube, S. Zimmermann, M. Steeb, R. Zengerle, P. Koltay, *Int. J. Mol. Sci.* **2015**, *16*, 16897.
[38] A. B. Rosenberg, C. M. Roco, R. A. Muscat, A. Kuchina, P. Sample, Z. Yao, L. T. Graybuck, D. J. Peeler, S. Mukherjee, W. Chen, S. H. Pun, D. L. Sellers, B. Tasic, G. Seelig, *Science* **2018**, *360*, 176.
[39] W. Gaisford, G. Schertler, P. Edwards, *Nat. Methods* **2011**, *8*, 520.

NANO MICRO small

Supporting Information

for *Small,* DOI: 10.1002/smll.201903739

Interfacial Nanoinjection-Based Nanoliter Single-Cell Analysis

Juanli Yun, Xiaowei Zheng, Peng Xu, Xu Zheng, Jingyue Xu, Chen Cao, Yusi Fu, Bingxue Xu, Xin Dai, Yi Wang, Hongtao Liu, Qiaolian Yi, Yaxin Zhu, Jian Wang, Li Wang, Zhiyang Dong, Li Huang, Yanyi Huang,* and Wenbin Du**

WILEY-VCH

Supporting Information (DOI: 10.1002/smll.201903739)

Interfacial Nanoinjection-Based Nanoliter Single-Cell Analysis

Juanli Yun[#], Xiaowei Zheng[#], Peng Xu[#†], Xu Zheng, Jingyue Xu, Chen Cao[‡], Yusi Fu, Bingxue Xu, Xin Dai, Yi Wang, Hongtao Liu, Qiaolian Yi, Yaxin Zhu, Jian Wang, Li Wang, Zhiyang Dong, Li Huang, Yanyi Huang*, Wenbin Du**

Dr. J.L. Yun, Dr. X.W. Zheng, Dr. P. Xu, J.Y. Xu, B.X Xu, Dr. X. Dai, Y. Wang, H.T. Liu, Q.L. Yi, Y.X. Zhu, Dr. J. Wang, Dr. L. Wang, Prof. Z.Y. Dong, Prof. L. Huang, Prof. W.B. Du

State Key Laboratory of Microbial Resources, Institute of Microbiology, Chinese Academy of Sciences, Beijing 100101, China

Prof. X. Zheng

State Key Laboratory of Nonlinear Mechanics, Institute of Mechanics, Chinese Academy of Sciences, Beijing 100190, China

Prof. Y.Y. Huang, Dr. C. Cao, Dr. Y.S. Fu

Biomedical Pioneering Innovation Center (BIOPIC), Beijing Advanced Innovation Center for Genomics (ICG), College of Engineering, School of Life Sciences, Peking-Tsinghua Center for Life Sciences, Peking University, Beijing 100871, China

J.Y. Xu, B.X. Xu, H.T. Liu, Q.L. Yi, Prof. Z.Y. Dong, Prof. L. Huang, Prof. W.B. Du

College of Life Sciences, University of the Chinese Academy of Sciences, Beijing 100049, China

Prof. W.B. Du

Savaid Medical School, University of the Chinese Academy of Sciences, Beijing 100049, China

# Dr. Juanli Yun, Dr. Peng Xu and Dr. Xiaowei Zheng contributed equally to this work.

* Corresponding authors: huangl@im.ac.cn (L. H.); huang@pku.edu.cn (Y. H.); wenbin@im.ac.cn (W. D.).

† Current address: Bioengineering and Therapeutic Sciences, University of California, San Francisco, San Francisco, CA 94158, USA

‡ Current address: Lewis-Sigler Institute for Integrative Genomics, Princeton University, Princeton, NJ 08540, USA

Experimental Section

Assembly of the Interfacial Nanoinjector (INJ). The INJ droplet handler contains a syringe pump (Pump 11 Pico Plus Elite, Harvard Apparatus, Holliston, MA, USA), an XYZ translation stage (PHOB-3, Zolix Instruments, Beijing, China), Teflon tubing (200 μm in O. D., 250 μm in I. D., Zeus, Orangeburg, SC, USA), a fused-silica capillary (187 μm in O. D., 50 μm in I. D., Polymicro Technologies, Phoenix, AZ, USA), the gas tight syringe (100 μL, Agilent, Santa Clara, CA, USA)and a commercially available 96- or 384-well plate (4346906 and 4309849, respectively, Applied Biosystems, Foster City, CA, USA).

To assemble the INJ liquid handler, a short silica-capillary (~20 mm) was fused with a lighter and cut to maintain a smooth tip-end, fused to a length adjustable Teflon tubing with wax, and then connected to a syringe. Reaction solution was then aspirated into the Teflon tubing by pulling the syringe slowly to avoid air bubbles in the solution. Before liquid generation and dispensing, the silica-capillary was first fixed on the translation stage (as shown in Figure S1), the silica-capillary was located to the center of the top-left microwell of the well-plate by control the translation stage. Mineral oil (M5094, Sigma Life Science, St. Louis, MO, USA) containing 0.01% Span-80 (1338-43-8, Sigma Life Science, St. Louis, MO, USA) was preloaded to the 96- or 384-well plate using pipette, 40 μL for 96- and 10 μL 384-well plate using a pipette, 40 μL in 96-well plates and 10 μL in 384-well plates. To generate the target volume nanoliter droplets, The pump and the translation stage were connected to a computer installed with the LabVIEW program (National Instrument, Austin, TX, USA), which generates various user-defined volumes. The translation stage panel is compatible with 96- and 384-well plates. A plate centrifuge (MINIP-2500, Miulab, Hangzhou, China) was used to accelerate the droplet deposition on the well bottom and the coalescence of different droplets.

Single-cell sorting, lysis, and gDNA amplification was performed in a HEPA-filtered environment conforming to Class 10000 cleanroom regulations. All the solutions in this work were automatically distributed with the INJ liquid handler in Vertical Laminar Flow Clean Benches (Gen 3, ESCO Ltd, Singapore).

The INJ liquid handler Evaluation. Different volumes of nanoliter droplets were generated with the INJ liquid handler, and the actual volumes of these droplets were measured under a microscope (Eclipse-Ti, Nikon, Tokyo, Japan). Different droplet volumes (0.5 nL, 1 nL, 2.5 nL, 5.0 nL, 7.5 nL, 10 nL and 20 nL) were generated and distributed to a flat bottom 96 well plate(3474, Corning Incorporated, Corning, NY, USA) preloaded with mineral oil using water dissolved blue pigment solution. The diameter of droplets were measured and their actual volumes were calculated accordingly. 40 droplets were generated and measured for each volume.

The pump-set volumes were 0.5 nL, 1 nL, 2.5 nL, 5.0 nL, 7.5 nL, 10 nL and 20 nL, and droplets were distributed in a flat-bottom 96-well plate preloaded with

mineral oil The diameter of the droplets was measured, and the actual volume was calculated. At least 50 droplets were measured for each volume.

Performance of droplet generation and coalescence. We evaluated the accuracy of INJ by comparing the target injection volume set on the pump with the droplet size measured from microscopy images. Figure 2c shows the linear regression between the theoretical and measured volumes. For the 5-nL target droplet volume, the measured volume was 4.9 ± 0.49 nL with a relative standard deviation (RSD) of 10% (n=40), indicating good precision and reproducibility (Movie S2). The INJ method avoids the disturbance of external forces such as acoustic ejection[1] and contamination due to surface contact or evaporation,[2] and allows single-cell assays to be scaled down to the tens of nanoliters level on standard well plates.

To evaluate the process of droplet coalescence, we used the chromogenic reaction for easy visualization of the bottom of the plate by eye (Figure 2d,e). To achieve reliable nanoliter coalescence, first, we use 96- or 384-well PCR plates with V-shaped bottoms to allow convergence of multiple droplets at the bottom of the well upon centrifugation; second, we preload the wells with mineral oil as the carrier oil because it is inert and biocompatible, and its low density (0.838 g/mL at 25°C) allows aqueous droplets to settle at the bottom of the well; third, we adjust the concentration of Span-80 in the mineral oil to obtain an optimal Span-80 concentration of 0.01% (v/v), which yields a coalescence ratio of 99.2% (n=288) for 5 nL droplets (Figure 2d, g). Moreover, at a Span-80 concentration of 0.02% (v/v), a 97.9% (n=288) coalescence ratio of the FACS-sorted droplets (~2 nL) with a preloaded 20-nL droplets further confirmed the effect of Span-80 for efficient droplet coalescence (Figure 2e, f). The possible mechanics of the Span-80 mediated nanoliter droplets coalescence is shown in Figure 2h,i,j.

Span-80 concentration optimization. A series of Span-80 concentration (0.000485%, 0.00145%, 0.00485%, 0.01%, 0.02%, 0.03%, 0.05, 0.1%, 0.2%, 0.5%, 0.6% and 1%) were used in this study to find the optimal Span-80 concentration for droplet coalescence. To visualize mixing of droplet contents once the droplet merged, a chromogenic reaction was used. In each well, two droplets using INJ were added sequentially, one of $FeCl_3$ (0.5 M, 5 nL) and the other of KSCN (0.1 M, 5 nL). Both droplets were colorless under the microscope. After centrifugation, the two droplets merged into one large droplet, which showed a visible red color due to the formation of the $Fe(SCN)_3$ complex (Figure 2d). We could easily calculate the coalescence ratio by directly observing the bottom of the wells and counting the red droplets before and after centrifugation. Using this method, we tested the optimal working concentration of Span-80 in mineral oil. Three 96-well plates were used for each concentration, and the coalescence ratio of each concentration was assessed. After the optimal Span-80 concentration was confirmed, the coalescence ratio of a FACS-generated 2 nL droplet with a 20 nL liquid handler generated droplet was further assessed using the FCl_3 and

KSCN color reaction and was compared with Span-80-free mineral oil, both with three 96-well plate replicates (Figure 2e).

FACS. The single-cell sorting by FACS is based on the DNA content (fluorescence) and scatter signals, which are related to cell size and granularity. Prior to FACS, cell suspensions were diluted to approximately 10^5 cells/mL with 1× phosphate-buffered saline (PBS). All samples were stained with the 1× SYBR Green DNA stain (S33102, Thermo Fisher Scientific, Waltham, MA, USA) for 10-20 min in the dark at 4°C. FACS was performed using a MoFlo XDP flow cytometer (Beckman Coulter, Brea, CA, USA) equipped with a 488 nm laser for excitation and a 100 μm nozzle orifice (Beckman Coulter, Brea, CA, USA). The cytometer was triggered by side scatter, and the "single-1 drop" mode was used for maximal sorting purity. Gates for the sorting of all cells were first defined based on light side scatter and then on particle green fluorescence, and finally on the single-cell sort gate (Figure S9). Cells were sorted into 96- or 384-well plates containing 40 μL or 10 μL of mineral oil (0.01% Span-80) as described above. All plates were centrifuged for 1 min immediately after sorting to spin the single-cell droplets down to the well bottom.

Single-cell culture and AST. A single colony of the *E. coli* ATCC25922 strain grown on LB agar was incubated in LB medium at 37°C overnight. The fresh cell culture was washed and diluted with 1×PBS to 10^5 cell/mL, stained with 1× SYBR Green and sorted into 384-well plates preloaded with LB containing 0.01% resazurin (20 nL to 100 nL). Single-cell culture was monitored by a plate reader (EnSpire, Perkin Elmer, Waltham, MA, USA) using fluorescence dynamics. The nonfluorescent dark cyan resazurin turns pink once the growth of cells occurs. The excitation and emission wavelengths for resazurin were 565 and 585 nm, respectively. Mineral oil containing Span-80 (10 μL) was added to each well of a 384-well plate. LB was also added to each well before sorting. Fluorescence dynamics were monitored for a continuous 16 h period, and data were collected every hour.

The AST of ampicillin against *E. coli* ATCC25922 was carried out by sorting bacteria cells into 384 wells, and incubating the cells in preloaded cation-adjusted Mueller-Hinton broth (CAMHB, 212322, BD, Franklin Lakes, NJ, USA) medium droplets with the indicated *ampicillin* concentrations. A serial dilution of ampicillin, 0, 0.125, 0.25, 0.5, 1, 2, 4, 8, 16, 32 and 64 μg/mL, was prepared and tested against single *E. coli* cells with a cultivation volume of 100 nL. Each concentration was repeated 72 times to allow the measurement of the ratio of growth inhibition at the single-cell level.

Single-cell genotyping of antibiotic-resistant bacteria. Single-cell antibiotic-resistance gene detection PCR was performed using a Quantstudio 5 qPCR thermocycler (Applied Biosystems, Foster City, CA, USA), and data were analyzed via ABI software. The PCR was performed by amplifying the antibiotic-resistance gene in the genome of single *A. baumannii* (ATCC19606) cells. A TaqMan probe targeting the beta-lactamase antibiotic resistance gene $bla_{\text{OXA-51}}$ was designed in this

study, and a 188 bp product of the *bla*$_{OXA-51}$ gene was amplified using the designed TaqMan probe and primers.

The *A. baumannii* strain was incubated at 37ºC overnight in LB medium. Cells were washed with PBS, stained with SYBR Green and sorted into 384-well plates (104 wells) through FACS. The parallel 15 μL volume single-cell reactions were carried out with 10 replicates; 10 (n=10) and 50 (n=10) cell PCRs were also performed. The PCR contained 2× ABI TaqMan Fast Advanced Master Mix (4444605, Applied Biosystems, Foster City, CA, USA), 250 nM of each primer, and 800 nM TaqMan probe. The primers for *bla*$_{OXA-51}$ gene were: forward, 5'-GCTGAACAACCCATCCAGTT-3'; reverse, 5'-TCAGCAAGAGGCACAGTTTG-3'. The TaqMan probe was 5'-FAM-TGGGTCTACATCCCATCCCCA-MGB-3'. Reaction mixes were prepared in a 20 μL volume and distributed in 384 microtiter plates with an INJ liquid handler. A 15 μL reaction mix was dispensed in each well using pipette tips. Since FACS-sorted droplets contain approximately 2 nL PBS, the 10 and 50 cell PCR mixes were prepared with reduced H_2O accordingly. The thermocycling protocol for qPCR consisted of an initial cell lysis step at 95°C for 5 min, followed by 50 cycles of 95°C for 10 s, 60°C for 20 s and elongation at 72°C for 20 s.

The bacteria strain *Pseudomonas aeruginosa* PAO1 that does not contain blaOXA-51 gene was used as negative control to evaluate the specificity of the PCR reaction. Cells were washed and sorted to 384-well plates according to the red fluorescent RFP plasmid in *P. aeruginosa* PAO1. The *bla*$_{OXA-51}$ gene targeted PCR was performed the same as in *A. baumannii* single cells described above with 80 replicates.

Single-cell gene expression profiling of mouse RAW264.7 macrophages by RT-PCR. The single cell gene expression in mammalian cells was carried out with Mouse RAW264.7 macrophage cells. Cells were purchased from ATCC and maintained in Dulbecco's modified Eagle's medium (DMEM, Invitrogen, Waltham, MA, USA) supplemented with 1% penicillin-streptomycin and 10% fetal bovine serum (FBS, HyClone, GE, Boston, MA, USA) at 37°C and 5% CO_2 in humidified air. Before RT-PCR, RAW264.7 cells were pretreated with 100 ng/mL LPS for 16 h. Cells treated with medium were used as a control.

For single-cell RT-PCR, fresh cells from both LPS-treated and untreated conditions were trypsinized to obtain cell suspensions, centrifuged at 4000 rpm for 5 min, and washed twice with PBS buffer. Dilution, staining and FACS were performed continuously as described above. After sorting, cells were centrifuged with 20 nL of preloaded lysis buffer (150343, Qiagen, Hilden, Germany), lysed at 65°C for 10 min, and neutralized with 20 nL of stop solution. RT-PCR was performed in final volumes of 200 nL, 400 nL, 600 nL, and 800 nL, with a TaqMan One-Step RT-qPCR kit (T2210, Solarbio, Beijing, China), each volume included 18 replicate wells. The RT-PCR mix contained 1× RT Mix, 25× Reaction Mix, 5× RT buffer, 800 nM of each

probe, 250 nM of each primer and filled with H_2O to a final volume of 25 μL. The reagents were distributed in 96-well plates with the INJ liquid handler at the designated volumes. The probe sequences for Hprt and IL-1β were as follows: Hprt probe 5'-FAM-ACCTAGATTTGTTTTGTATACCT-MGB-3'; IL-1β probe 5'-VIC-AGAGCATCCAGCTTC-MGB-3'. Primers for IL-1β were: forward, 5'-TTGAAGTTGACGGACCCCA-3'; reverse, 5'-ATGAGTGATACTGCCTGCCTGA-3'. RT-PCR was performed with the one-step RT program: 50°C for 30 min for reverse transcription, followed by 50 cycles of 95°C for 15 s and 60°C for 30 s. The fluorescence dynamics were measured with a Viia7 96 Real-Time PCR thermocycler (Applied Biosystems, Foster City, CA, USA). The mRNA levels of Hprt and IL-1β were measured. Data were analyzed using the Viia7 Real-Time PCR system software.

Single-cell WGA. To perform single-cell WGA on *Sulfolobus* sp. A20, the strain was grown at 75°C with shaking in Zillig's medium.[3] Cells were collected at an OD_{600} of 0.4~0.6 by centrifugation and washed three times with sterilized PBS. were then prepared as described above in the FACS section. After single-cell sorting, 20 nL of lysis buffer was added to the well, the plate centrifuged and cells lysed in a metal bath at 65°C for 10 min. The lysis was terminated by the addition of 20 nL of stop solution to each well, followed by centrifugation for 1 min to allow coalescence. MDA reaction mixtures were prepared in specified volumes according to the QIAGEN REPLI-g Single cell kit (150343, Qiagen, Hilden, Germany) and were distributed using INJ liquid handler with the optimal reaction volumes (360 nL~560 nL). We also used a normal volume (10 μL, n=3) reaction to compare its amplification efficiency with that of our nanoliter amplification method. Fluorescence data were automatically collected every 10 min with an ABI Viia7 real-time PCR thermal cycler. After genome amplification, microwells containing successfully amplified products were diluted with 20 μL nuclease-free water with pipette tips, centrifuged to separate with mineral oil, and then transferred into clean 0.2 mL PCR tubes with pipette. PCR tubes were centrifuged again to spin down the nucleic acid solution to the well bottom. There might be a thin layer of mineral oil in the surface of the nucleic acid aqueous, which will not affect the following analyses such as PCR due to the bio-compatibility of the mineral oil.

To perform single-cell WGA on prokaryotic cells from environmental samples, a sample (5 g) of deep-sea sediment from the Southwest Indian Ocean was resuspended in 1 × PBS buffer (10 mL), vortexed and centrifuged at 2500 × g for 1 min to remove large particles. The preparation and MDA amplification of environmental microbes were performed the same as *Sulfolobus* A20. Nuclease-free water (20 μL) was added to the amplicon droplets as described above in the benchmark strain *Sulfolobus* A20, transferred to new PCR tubes and used for the next-step PCR identification. An aliquot (1 μL) of each product was used for PCR-based 16S rRNA gene identification with 515F (5'-GTGYCAGCMGCCGCGGTAA-3') and 1406R (5'-GACGGGCGGTGWGTRCAA-3') primers for each amplicon. The MDA

products with the right 16S rRNA gene PCR products were sequenced and blasted in the NCBI blast online website (https://blast.ncbi.nlm.nih.gov) to find their phylogeny assignment, only MDA products that with interested 16S rRNA gene detected were sent for whole genome sequencing and analysed.

We have tested the evaporation problem during the experiments, we found that droplets in the well plates can be stored at 4ºC for a week and at least one month at -20ºC. When large numbers of samples were processed, we suggest deposit amplification products under -80ºC for longer storage.

The lysis of yeast cells or fungi spores can be lysed using a combination of enzymatic and alkaline solutions according to a reference.[4] Briefly, solutions were prepared with the following reagents: KOH dry pellets (reconstituted to 500mM with nuclease-free water), 1M dithiothreitol, and HCl (Stop Buffer) were obtained from the REPLI-g WGA Single-Cell Kit (150345, Qiagen); Tween 20 (P9416-100ml, Sigma)); 0.5M EDTA (AM92606, Ambion); proteinase K (P8107S, NEB); phenylmethylsulfonyl fluoride (532789-5 g, Sigma); and EGTA (E3889-10 g, Sigma).

Sequencing and SCG assembly. All single-cell MDA amplicons in this work were sequenced using an Illumina HiSeq 2000 system in 2× 150 bp mode at AnnoGenne, Beijing, China. In total, 2 Gb of paired end reads were generated for each single-cell amplicon. The sequence reads were quality-trimmed with Trimmomatic [5] with the following options: LEADING: 3 TRAILING: 3 SLIDINGWINDOW: 4:15 and MINLEN: 36. High-quality reads were assembled with SPAdes [6] single-cell mode with the following settings: --careful --sc --phred-offset 33. All assembled single-cell genome scaffolds were evaluated with QUAST. [7] Basic mapping and chimera statistics were obtained using SAMtools [8] on the mapped reads. After the removal of reads with mapping quality scores less than 30 from the created SAM files, genome coverage was calculated with the aligned reads using BEDTools. [9] The uniformity of the reads was analyzed by Deeptools [10] with a binning size of 1000 bp.

A rarefaction analysis was carried out to determine the optimal sequencing depth for benchmark and environmental bacterial SCGs. The reads were randomly downsampled to 1×, 5×, 10×, 20×, 50×, 100×, 300×, 500×, 800×, and 1000× depth per assembly. Mapping of the sequencing reads for *Sulfolobus* sp. A20 was performed by Bowtie2,[11] and unmapped reads were extracted using Samtools and blasted with Blast^{+} [12] using a database downloaded from NCBI. The contamination of the A20 SCG assemblies was assessed using CheckM [13] with the lineage-specific workflow and default parameters.

The SSU rRNA sequences were predicted and retrieved from environmental assemblies using Barrnap (https://github.com/tseemann/barrnap). 16S rRNA gene sequences were used for phylogenetic assignments and phylogenetic tree construction. The maximum likelihood phylogenetic tree was built using Mega 7. [14] Assembled scaffolds were sent to RAST online server. [15] The completeness and contamination

of the marine sediment SCG assemblies was assessed using CheckM [13] with the lineage-specific workflow and default parameters. CAZymes in each genome assembly were annotated by the online CAZy database http://csbl.bmb.uga.edu/dbCAN/.

Data deposits. All sequencing and assembled genome data were deposited in NCBI GenBank SRA under accession numbers SRP150301 and SRP152691. Single-cell genomes were deposited at DDBJ/ENA/GenBank and are provided in Supplementary Table 2.

References

[1] J. Olechno, R. Stearns, R. Ellson, E. Heron, *Innov. Pharm. Technol.*, **2006**, *19*, 40.

[2] W. Gaisford, G. Schertler, P. Edwards, *Nat. Methods*, **2011**, *8*.

[3] X. Dai, H. Wang, Z. Zhang, K. Li, X. Zhang, M. Mora-Lopez, C. Jiang, C. Liu, L. Wang, Y. Zhu, W. Hernandez-Ascencio, Z. Dong, L. Huang, *Front. Microbiol.*, **2016**, *7*, 1902.

[4] S. R. Ahrendt, C. A. Quandt, D. Ciobanu, A. Clum, A. Salamov, B. Andreopoulos, J. F. Cheng, T. Woyke, A. Pelin, B. Henrissat, N. K. Reynolds, G. L. Benny, M. E. Smith, T. Y. James, I. V. Grigoriev, *Nat. Microbiol.*, **2018**, *3*, 1417.

[5] A. M. Bolger, M. Lohse, B. Usadel, *Bioinformatics*, **2014**, *30*, 2114.

[6] A. Bankevich, S. Nurk, D. Antipov, A. A. Gurevich, M. Dvorkin, A. S. Kulikov, V. M. Lesin, S. I. Nikolenko, S. Pham, A. D. Prjibelski, A. V. Pyshkin, A. V. Sirotkin, N. Vyahhi, G. Tesler, M. A. Alekseyev, P. A. Pevzner, *J. Comput. Biol.*, **2012**, *19*, 455.

[7] A. Gurevich, V. Saveliev, N. Vyahhi, G. Tesler, *Bioinformatics*, **2013**, *29*, 1072.

[8] H. Li, B. Handsaker, A. Wysoker, T. Fennell, J. Ruan, N. Homer, G. Marth, G. Abecasis, R. Durbin, *Bioinformatics*, **2009**, *25*, 2078.

[9] A. R. Quinlan, I. M. Hall, *Bioinformatics*, **2010**, *26*, 841.

[10] F. Ramirez, F. Dundar, S. Diehl, B. A. Gruning, T. Manke, *Nucleic Acids Res.*, **2014**, *42*, W187.

[11] B. Langmead, S. L. Salzberg, *Nat. Methods*, **2012**, *9*, 357.

[12] P. Santiago-Sotelo, J. H. Ramirez-Prado, *Biotechniques*, **2012**, *53*, 299.

[13] D. H. Parks, M. Imelfort, C. T. Skennerton, P. Hugenholtz, G. W. Tyson, *Genome Res.*, **2015**, *25*, 1043.

[14] S. Kumar, G. Stecher, K. Tamura, *Mol. Biol. Evol.*, **2016**, *33*, 1870.

[15] R. K. Aziz, D. Bartels, A. A. Best, M. DeJongh, T. Disz, R. A. Edwards, K. Formsma, S. Gerdes, E. M. Glass, M. Kubal, F. Meyer, G. J. Olsen, R. Olson, A. L. Osterman, R. A. Overbeek, L. K. McNeil, D. Paarmann, T. Paczian, B. Parrello, G. D. Pusch, C. Reich, R. Stevens, O. Vassieva, V. Vonstein, A. Wilke, O. Zagnitko, *Bmc Genomics*, **2008**, *9*, 75.

Table S1 Annotation details of the benchmark strain *Sufolobus* sp. A20 assemblies

Sample ID	Total length (Mb)	Largest contig (bp)	Number of contigs	GC (%)	N50 (bp)	Coverage (%)	Contamination （%）
10 µl-F6	2.58	121804	435	32.23	20352	72.9	27.5
10 µl-F8	3.03	108053	443	33.43	26071	93.6	28.83
10 µl-G8	1.99	51205	865	34.13	6986	82.5	33.1
360 nL-B1-3	2.08	63283	524	35.89	10994	67.0	24.69
360 nL-E1-3	2.41	98875	297	34.79	21135	86.0	0.63
360 nL-F1-3	2.41	60390	338	34.84	19767	83.8	0.89
460 nL-C3-3	2.37	96394	272	34.85	24824	83.3	1.79
460 nL-E3-3	1.39	27131	437	34.83	6045	46.6	4.96
460 nL-F3-3	1.53	25452	521	35.01	5481	49.7	0.93
560 nL-B5-3	2.22	71739	430	34.92	14262	74.3	1.19
560 nL-D5-3	1.85	52948	405	34.74	10403	62.9	4.61
560 nL-E5-3	1.49	38439	389	34.85	9014	52.8	0.79

Table S2 The completeness and contamination ratio of the Southwest Indian Sea sediments microorganism assemblies

Sample ID	Completeness (%)	Contamination (%)
G-1	11.9	0.00
G-2	27.0	0.00
G-3	15.0	1.64
G-4	7.68	0.00
G-5	73.5	2.07
G-6	52.6	0.59
G-7	27.8	0.67
T-1	55.4	0.98
T-2	12.5	0.00
T-3	28.4	0.00
T-4	33.4	0.04
T-5	32.1	3.59
T-6	6.04	0.43
T-7	26.9	3.09
T-8	32.0	2.46
T-9	16.3	1.36

Table S3 Accession numbers of the assembled single-cell genomes in this study

Sample ID	Sample origin	Accession number	Affiliations
G-1	Sediment G	PYVL00000000	*Methylophaga nitratireducenticrescens*
G-2	Sediment G	PYVK00000000	*Sulfurovum lithotrophicum*
G-3	Sediment G	PYVJ00000000	*Uncultured cyanobacterium*
G-4	Sediment G	PYVI00000000	*Alcanivorax venustensis*
G-5	Sediment G	PYVH00000000	*Marinobacter*
G-6	Sediment G	PYVG00000000	*Idiomarina aestuarii*
G-7	Sediment G	PYVF00000000	*Idiomarina aestuarii*
T-1	Sediment T	PYVU00000000	*Marivirga lumbricoides*
T-2	Sediment T	PYVT00000000	*Marinobacter*
T-3	Sediment T	PYVS00000000	*Idiomarina aestuarii*
T-4	Sediment T	PYVR00000000	*Idiomarina aestuarii*
T-5	Sediment T	PYVQ00000000	*Marinobacter*
T-6	Sediment T	PYVP00000000	*Marinobacter vinifirmus*
T-6	Sediment T	PYVO00000000	*Thalassospira xiamenensis*
T-7	Sediment T	PYVN00000000	*Idiomarina aestuarii*
T-8	Sediment T	PYVM00000000	*Idiomarina aestuarii*
T-9	Sediment T	PYVU00000000	*Marivirga lumbricoides*
10 μl-F6	*Sulfolobus* sp. A20	SAMN09205297	*Sulfolobus* sp. A20
10 μL-F8	*Sulfolobus* sp. A20	SAMN09205298	*Sulfolobus* sp. A20
10 μL-G8	*Sulfolobus* sp. A20	SAMN09205299	*Sulfolobus* sp. A20
360 nL-B1-3	*Sulfolobus* sp. A20	SAMN09205290	*Sulfolobus* sp. A20
360 nL-E1-3	*Sulfolobus* sp. A20	SAMN09205288	*Sulfolobus* sp. A20
360 nL-F1-3	*Sulfolobus* sp. A20	SAMN09205289	*Sulfolobus* sp. A20
460 nL-C3-3	*Sulfolobus* sp. A20	SAMN09205293	*Sulfolobus* sp. A20
460 nL-E3-3	*Sulfolobus* sp. A20	SAMN09205291	*Sulfolobus* sp. A20
460 nL-F3-3	*Sulfolobus* sp. A20	SAMN09205292	*Sulfolobus* sp. A20
560 nL-B5-3	*Sulfolobus* sp. A20	SAMN09205295	*Sulfolobus* sp. A20
560 nL-D5-3	*Sulfolobus* sp. A20	SAMN09205296	*Sulfolobus* sp. A20
560 nL-E5-3	*Sulfolobus* sp. A20	SAMN09205294	*Sulfolobus* sp. A20

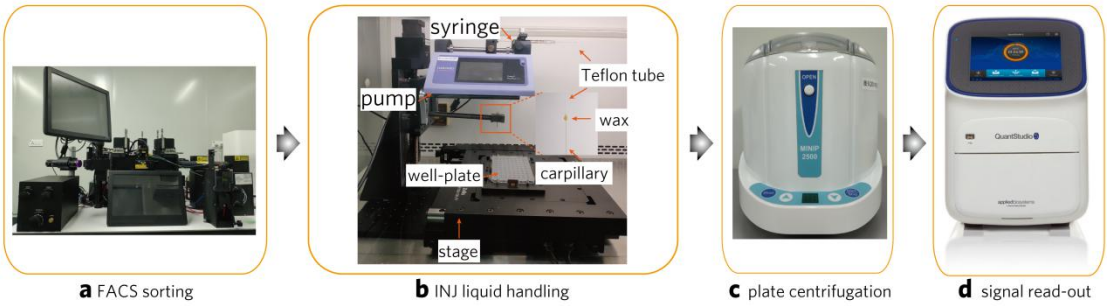

Figure S1 Photo of the FACS-INJ pipeline which contains a) the flow cytometer, b) the INJ droplet handler, c) the plate centrifuge and d) the common fluorescence reader such as real-time PCR machine.

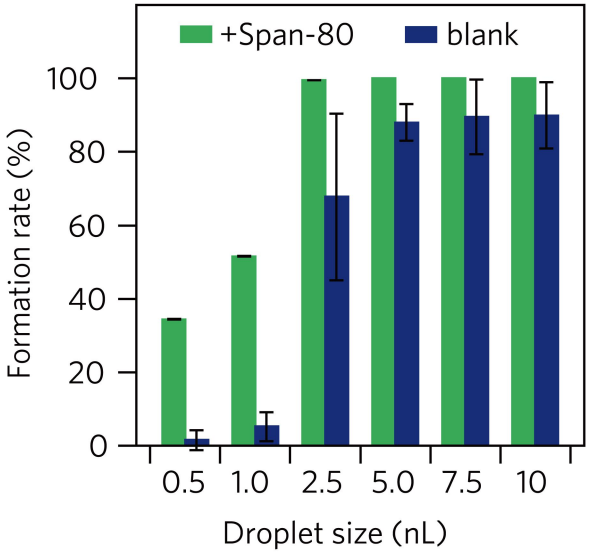

Figure S2 Droplet formation rate with different droplet sizes. The number of successfully formed droplets was counted, and the droplet formation rate was calculated. All droplets were generated using the INJ droplet handler, with or without Span-80 (0.02%). Error bars are the standard deviation of 96 droplets.

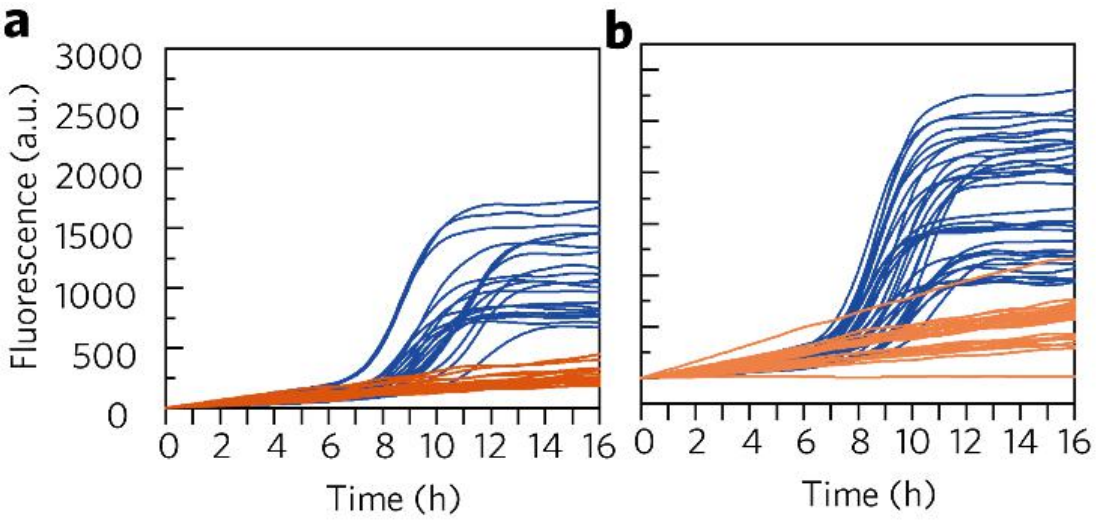

Figure S3 *E. coli* single-cell culture volume optimization in a) 20 nL and b) 50 nL reaction volumes. The 100 nL volume shows the best amplification results according to the fluorescence curve used in AST (Figure 3b).

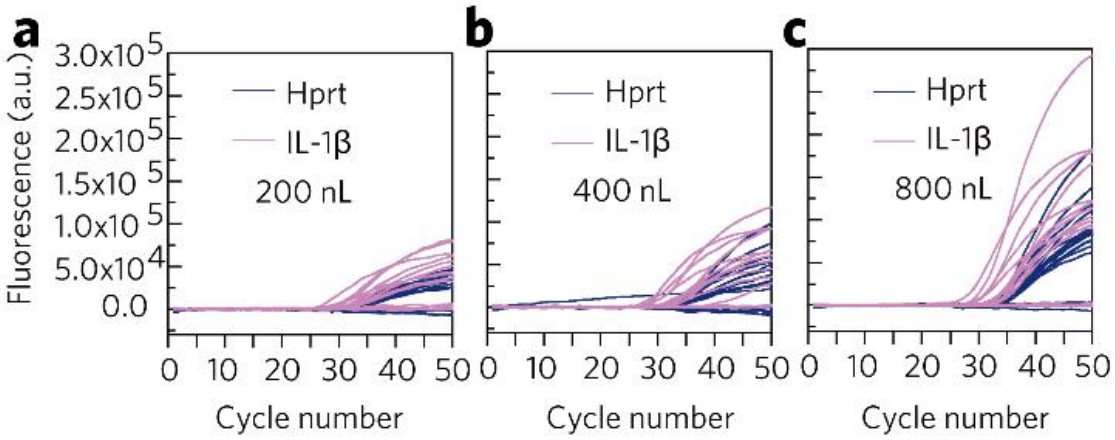

Figure S4 Mammalian single-cell RT-PCR volume optimization in a) 200 nL, b) 400 nL and c) 800 nL reaction volumes. The 600 nL volume showed the best amplification results according to the fluorescence curve and was used in RT-PCRs (Figure 5b).

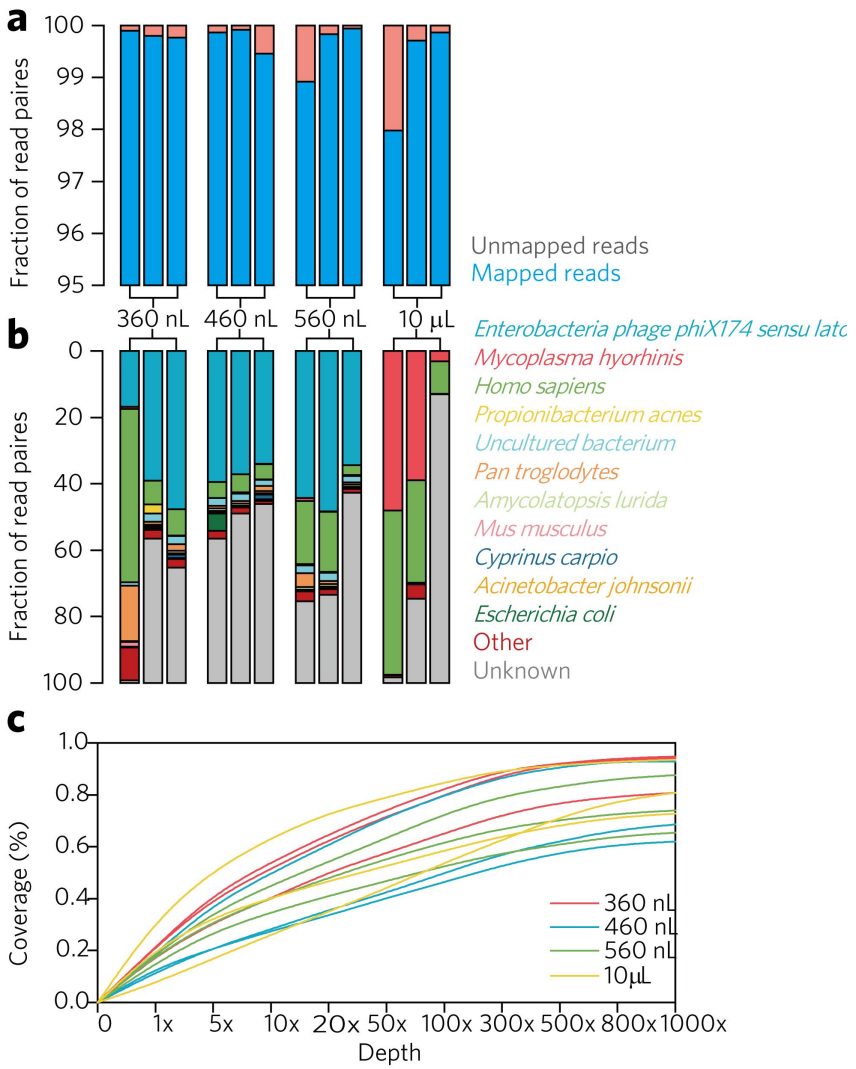

Figure S5 Sequencing read mapping quality and depth in single cells of the benchmark strain *Sulfolobus* sp. A20. a) The proportion of mapped and unmapped reads calculated by mapping the sequencing reads to the corresponding single-cell assembly. b) The taxonomic assignment of unmapped reads using 10000 randomly selected reads. c) Genome coverage of each assembly according to the sequencing depth.

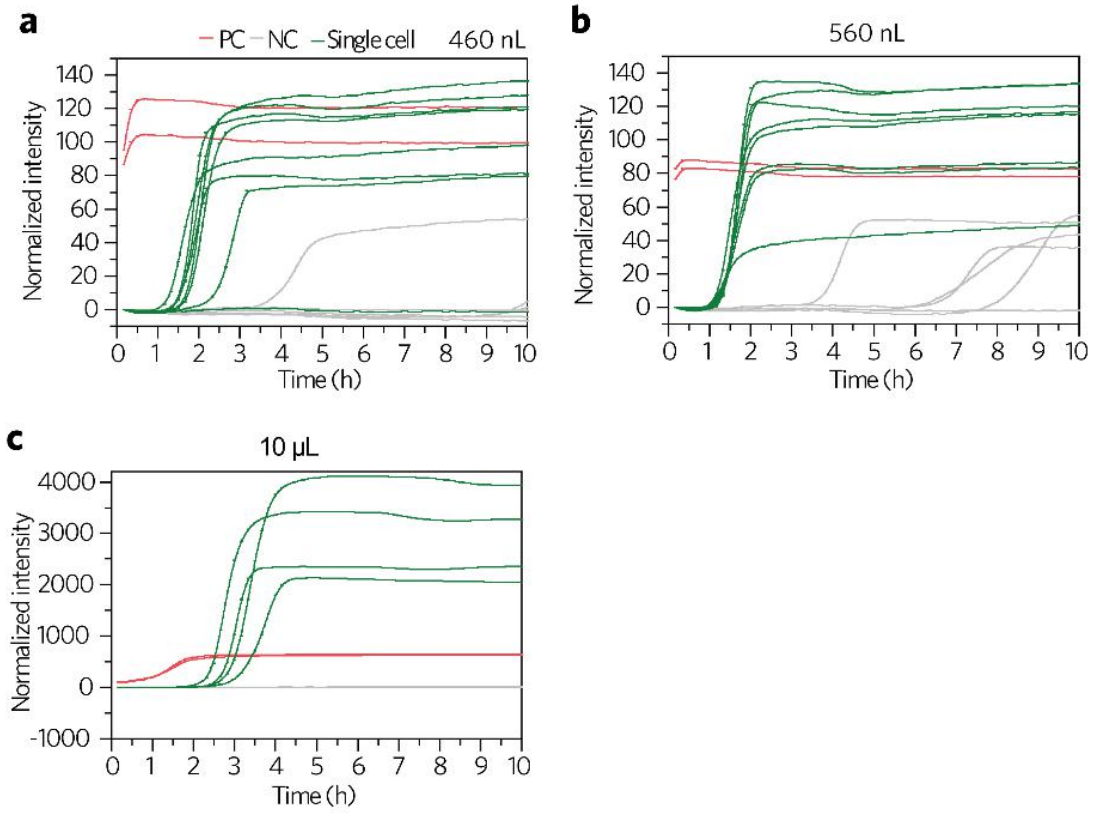

Figure S6 Nanoliter MDA amplification curves in a) 460 nL b) 560 nL and c) 10 µL volumes. PC: positive control with 100 cells; NC: negative controls; Single cell, one cell.

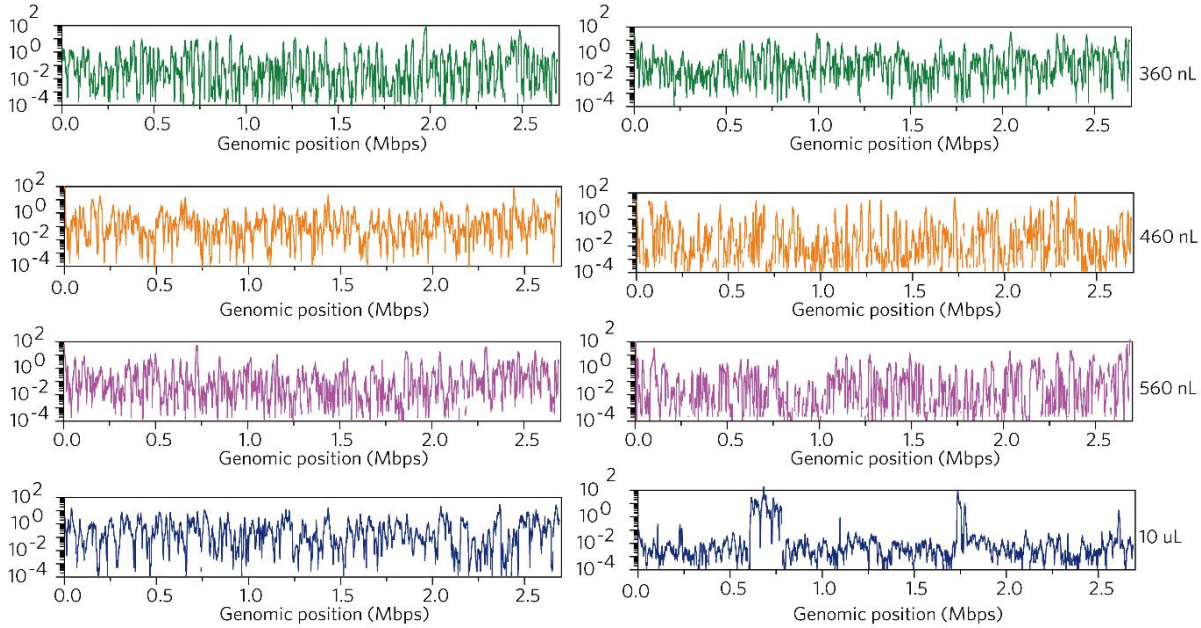

Figure S7 The uniformity of *Sulfolobus* sp. A20 single-cell genome assemblies in different MDA reaction volumes.

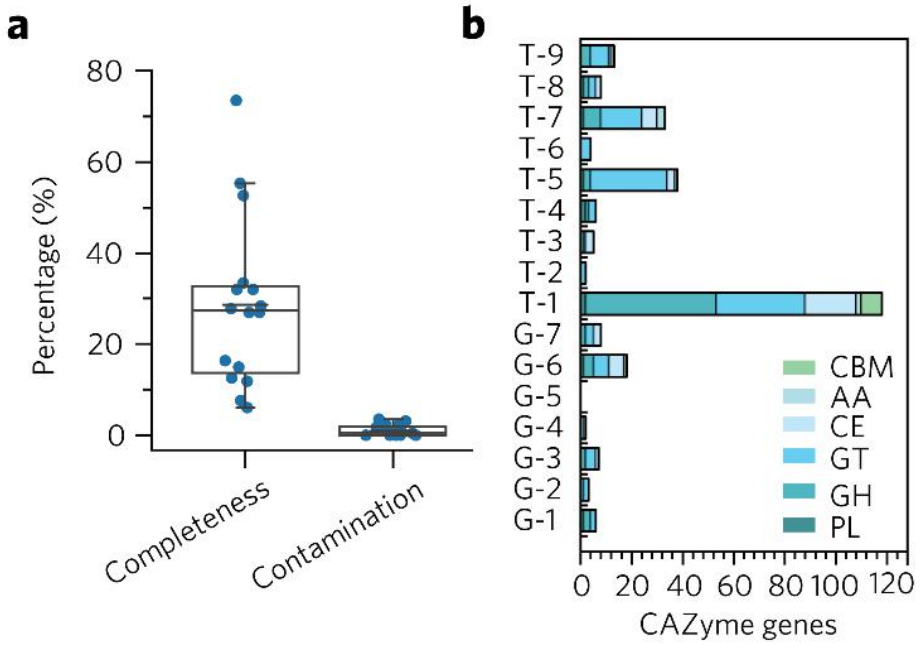

Figure S8 Quality and functional annotation of genome assemblies of single microbial cells from the Southwest Indian sea sediments. a) The completeness and contamination ratio of the single-cell genome assemblies, assessed by CheckM. b) Carbohydrate-active enzymes detected in the single-cell assemblies, annotated by the online CAZy database (http://csbl.bmb.uga.edu/dbCAN/).

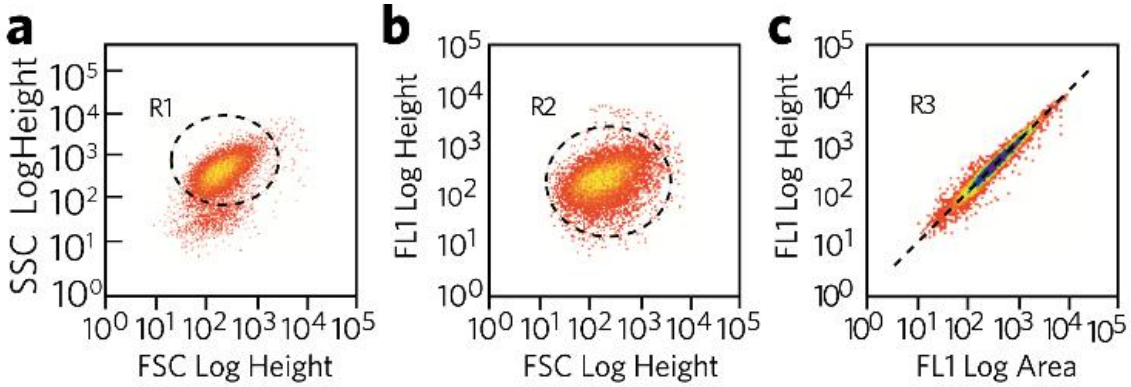

Figure S9 The FACS logic used in single-cell sorting. Cells were first selected by a) particle size, then b) fluorescence intensity and finally c) the single-cell mode linear scatter principle.

Movie S1. Real-time movie of sequential interfacial nanoinjection (INJ) of 1 nL, 5 nL, 10 nL, 20 nL, 50 nL and 100 nL droplets in a glass reservoir preloaded with mineral oil.

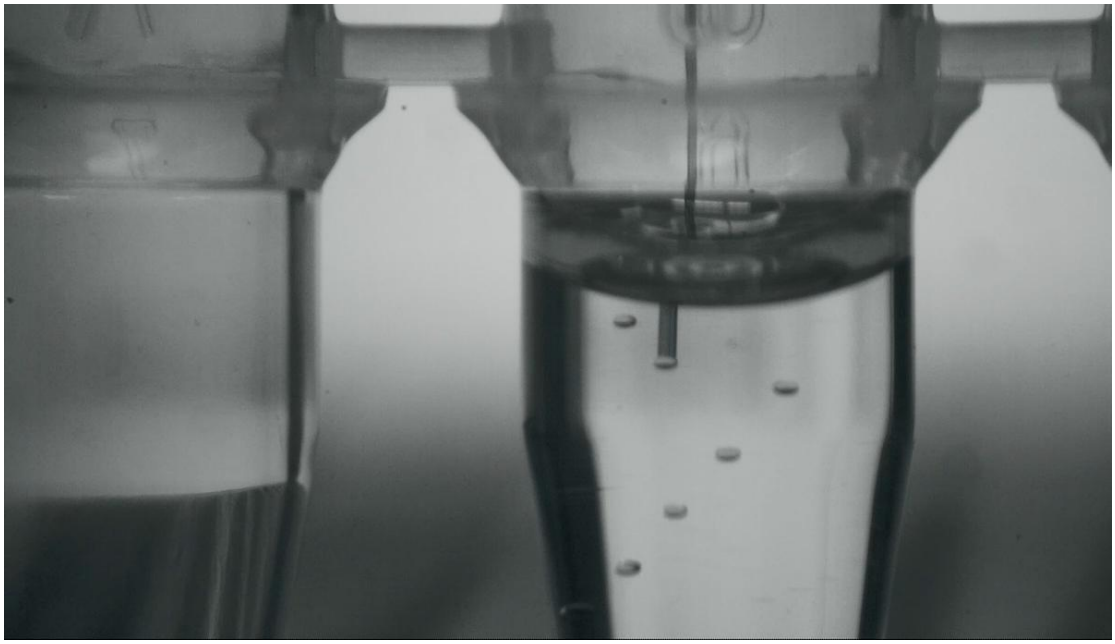

Movie S2. Continuous interfacial nanoinjection (INJ) of 5 nL droplets in a 100-µL PCR tube. The tube was preloaded with mineral oil.